Article

Numerical Simulation of Wormhole Propagation with Foamed-Viscoelastic-Surfactant Acid in Carbonate Acidizing

Lufeng Zhang [1,2,*], **Haibo Wang** [1,2], **Fujian Zhou** [3,*] **and Jianye Mou** [3]

1   Key Laboratory of Marine Oil & Gas Reservoirs Production, Sinopec Petroleum Exploration and Production Research Institute, Beijing 100083, China; wanghaibo.syky@sinopec.com
2   State Energy Center for Shale Oil Research and Development, Beijing 100083, China
3   College of Petroleum Engineering, China University of Petroleum, Beijing 100083, China
*   Correspondence: zlfcupb@163.com (L.Z.); zhoufj@cup.edu.cn (F.Z.)

Abstract: Successful matrix acidizing for extremely thick carbonate reservoirs with long horizontal well sections and strong heterogeneity requires efficient temporary plugging and diverting of acid fluid, ensuring acid fluid distribution to each production layer. Foamed-viscoelastic-surfactant (Foamed-VES) acid combines the benefits of both foam acid and viscoelastic surfactant (VES) acid, integrating foam plugging and viscous plugging. It can achieve uniform acid distribution in highly heterogeneous reservoirs. However, little research has been conducted on the wormhole propagation law of foamed-VES acid. To address this gap, this study established a mathematical model of foamed-VES acid wormhole propagation based on the dual-scale model. The model was coupled with a random porosity distribution generated with geological statistical software. The effects of different factors on foamed-VES acid etching were simulated. Numerical results show that foamed-VES acid can stimulate low-permeability reservoirs with a permeability differential of 20. Its inherent mechanism lies in the synergy of foam plugging and VES viscous plugging. This study enhances our understanding of the acid diversion mechanism of foamed-VES acid, providing a theoretical foundation for on-site acidizing treatment.

Keywords: carbonate reservoir; temporary plugging and diverting; foamed-VES acid

1. Introduction

The recently published 2022 Energy Outlook report by the U.S. Energy Information Administration (EIA) reveals that more than 60% of the world's oil and 40% of the world's gas are stored in carbonate reservoirs [1]. However, increasing demand for oil and gas energy and the development of carbonate reservoirs have forced petroleum engineers to tap oil and gas reserves with poor physical properties, such as strong reservoir heterogeneity, high temperatures, and natural fracture development [2–4]. Unfortunately, developing these reserves has become increasingly challenging and expensive.

Matrix acidizing is a highly effective and indispensable technology for economically developing carbonate reservoirs. It involves injectin acid fluids, such as hydrochloric acid, thickened acid, or foam acid, into the formation below fracture pressure to dissolve carbonate minerals, creating acid wormholes that penetrate contamination zones, communicate with distant reservoirs and natural fractures, and restore oil and gas well productivity [5–7]. The success of acidizing operations depends on the ability to distribute the acid uniformly in the reservoir. The conventional matrix acidizing technique encounters difficulties when dealing with very thick layers or long, horizontal well sections with strong heterogeneity, as acid flow always favors low seepage resistance paths, resulting in insufficient reservoir utilization and unsatisfactory stimulation effects [8].

One of the most widely used chemical diverting agents currently is the self-diverting acid based on VES. It is interesting to note that VES acid can undergo self-viscosification through the reaction between acid and carbonate rock. In the presence of divalent calcium

ions, VES molecules entangle spherical micelles to form wormlike micelles, which can significantly increase the viscosity of spent acids. During VES acidizing treatment, the self-viscosification process occurs first in the high-permeability layer, where there is less resistance to VES acid. This forces the subsequently injected VES acid into other low-permeability layers, resulting in the uniform distribution of acid. Furthermore, viscosified VES acid breaks upon encountering hydrocarbons and flows back without causing any formation damage [9–12]. Due to its excellent cleaning properties and lack of pollutant byproducts, VES has gained widespread acceptance in the industry. However, for some older oilfields with low formation pressures and enhanced reservoir heterogeneity resulting from previous acidization, as well as for production wells in water-injected fields with high water saturations, the diversion effect of VES acid is not obvious [13,14].

Foam has been developed as another chemical method to serve as a diverting agent in acidizing, with research tracing back to 1969 [15]. Since then, numerous experimental and numerical simulation studies have been conducted to investigate the various factors that influence foam-diverting acidizing, including initial permeability, permeability contrast, foam quality, saturation condition, injection rate, and foam rheological behavior [16–19]. From these studies, foam acidizing has been found to have several advantages. Firstly, foam selectively plugs high-permeability layers more effectively than low-permeability layers. This allows for the stimulation of low-permeability layers, thereby enhancing the effect of acidizing treatment. Secondly, foam fluid has selective effects on oil and water layers, with acid preferentially stimulating the oil layer. Thirdly, the energy provided by the expansion of gas in the foam facilitates residual acid flow back, reducing residual damage. Finally, foam acid is a retard acid that reduces the acid-rock reaction rate and achieves deep acidizing. However, foamed acid also has some limitations, including poor temperature resistance, complex formula, and a lack of effectiveness under high-permeability contrast, which limits its further application [20].

To overcome the limitations of foam and VES acid, foam-based VES acid has been developed and applied successfully on site, harnessing the characteristic of foam to "plug large pores without blocking small ones, and block water without blocking oil" [21], combined with the excellent properties of VES. Although the application effect of foam-based VES acid in the field is excellent, little is known about its diverting mechanism and influencing factors.

2. Mathematical Model

In this section, a mathematical model is developed based on the average continuity model (dual-scale) to simulate the propagation of wormholes for foamed VES [22]. The newly developed model includes not only the Darcy scale and pore scale models but also the foam-VES acid rheology model, which sets it apart from the conventional Panga dual-scale model. Furthermore, when establishing the model, sink terms, inertial forces, gravity, and compressibility effects of formation fluids and rocks are neglected for the sake of simplification.

2.1. Darcy Scale Model

The Darcy scale model mainly consists of the continuity equation, the motion equation, the acid mass balance equation, and other equations.

Typically, the continuity equation is derived by choosing small control volumes and is based on the principle of conservation of fluid mass. In accordance with the fluid mass conservation equation, the inflow plus the outflow, plus any source or sink terms, equals the cumulative change in mass over time:

$$\frac{\partial(\rho \boldsymbol{u_x})}{\partial x} + \frac{\partial(\rho \boldsymbol{u_y})}{\partial y} + \frac{\partial(\rho \boldsymbol{u_z})}{\partial z} + \frac{\partial(\rho \varphi)}{\partial t} = 0 \tag{1}$$

where ρ is the density of foamed-VES acid, kg/m^3; ϕ is the original porosity of the formation, %.

The Darcy–Brinkman equation [23] has wide applicability, as it is capable of describing the flow of acid in the matrix, wormholes, and fractures simultaneously. This equation can thus be effectively utilized to describe fluid flow during the acidification of fractured carbonate reservoirs, thereby enabling the distribution of the reaction pressure field to be determined.

$$\mu k^{-1} u + \nabla \boldsymbol{p} - \mu \Delta u = 0 \tag{2}$$

where $\boldsymbol{p}$ is the formation pressure, MPa; μ is the viscosity of foamed-VES acid, in Pa·s; k is formation permeability, μm^2; u is the velocity tensor, dimensionless.

Foamed-VES acid undergoes a reaction with carbonate minerals upon entering the reservoir and is subsequently influenced by convection and diffusion. As a result, the substance concentration in the foamed-VES acid solution decreases with the flow, and the derived concentration balance equation for foamed-VES acid can be expressed as follows:

$$\nabla(\phi D_e \cdot \nabla C_f) - \nabla(U C_f) - k_c a_v (C_f - C_s) = \frac{\partial(\phi C_f)}{\partial t} \tag{3}$$

where D_e is the effective diffusion coefficient of foamed-VES acid solution, m^2/s; C_f is the concentration of foamed-VES acid solution, mol/L. k_c is the mass transfer coefficient of foamed-VES acid solution, m/s; C_s is the concentration of foamed-VES solution on the surface of porous media, mol/L; k_s is the reaction rate constant of foamed-VES acid, m/s.

The concentration of calcium ions and viscoelastic surfactants has a certain impact on the acidification effect, and the specific equation is as follows:

$$\nabla(\phi D_e \cdot \nabla C_{Ca^{2+}}) - \nabla(U C_{Ca^{2+}}) - k_c a_v (C_f - C_s) = \frac{\partial(\phi C_{Ca^{2+}})}{\partial t} \tag{4}$$

$$\nabla(\phi D_e \cdot \nabla C_{VES}) - \nabla(U C_{VES}) = \frac{\partial(\phi C_{VES})}{\partial t} \tag{5}$$

where C_{Ca}^{2+} is the calcium ion concentration in the pore medium after acid rock reaction, mol/L. C_{VES} is the concentration of viscoelastic surfactant in acid solution, mol/L.

2.2. Pore Scale Model

In order to solve the equations in the Darcy scale model, certain physical parameters of the reservoir (such as rock-specific surface, reservoir porosity, permeability) and the mass transfer coefficient of foamed-VES acid need to be utilized. However, these parameter values are largely dependent on the pore structure of the reservoir. Quantifying the precise relationship between these parameters and pore structure is challenging; therefore, semi-empirical formulas are typically used to approximate this relationship.

Describe changes in reservoir permeability:

$$\frac{K}{K_0} = \frac{\phi}{\phi_0} \left(\frac{\phi}{\phi_0} \left(\frac{1 - \phi_0}{1 - \phi} \right) \right)^{2\beta} \tag{6}$$

Describe the variation in reservoir pore radius:

$$\frac{r_P}{r_{p0}} = \sqrt{\frac{K \phi_0}{\phi K_0}} \tag{7}$$

Describe the change in rock-specific surface area:

$$\frac{a_v}{a_0} = \frac{\phi r_{p0}}{\phi_0 r_p} \tag{8}$$

Describe the mass transfer and diffusion coefficient of acid solution:

$$Sh = \frac{2k_c r_p}{D_m} = Sh_\infty + \frac{0.7}{h^{1/2}} Re_p^{1/2} Sc^{1/3} \tag{9}$$

$$D_{eX} = \alpha_{os} D_m + \frac{2\lambda_x \left|\vec{U}\right| r_p}{\phi} \tag{10}$$

$$D_{eY} = \alpha_{os} D_m + \frac{2\lambda_T \left|\vec{U}\right| r_p}{\phi} \tag{11}$$

where φ and φ_0 represent the formation porosity and the initial porosity, respectively, %; r_p and r_{p0} are pore radius and initial pore radius, respectively, m; K and K_0 represent reservoir permeability and initial permeability, respectively, μm^2; β represents the relationship between permeability and porosity, constant dimensionless; a_0 represents the initial specific surface area of rock, m^{-1}; Sh is Sherwood number, indicating the ratio of convection mass transfer and diffusion mass transfer of acid solution; Sh_∞ is the asymptotic Sherwood number, which is generally taken as 2; D_m is the effective diffusion coefficient, m^2/s; H represents the ratio of length to the diameter of porous media, dimensionless; Re_p is the Reynolds number; Sc is the ratio of the effective viscosity to the effective diffusion coefficient of the acid solution; λ_x, λ_T, and α_{os} are constants of connection with reservoir pores.

2.3. Rheological Model

To accurately simulate the acidification flow of foamed VES, constructing a comprehensive rheological model is crucial. Currently, empirical formulas are almost exclusively used to describe the complex rheological properties of foam fluids [24]. As the power-law model is commonly used in the characterization of fracturing fluids, a similar approach can be employed in the development of a power-law rheological model for foam-based acid. For each acid solution with different foam qualities, a customized power-law function can be obtained by fitting the coefficients and exponents to the foam quality. This leads to the development of an empirical rheological formula for foam-based acid that incorporates foam quality.

$$\mu_F = (679.31 + 186.14e^{\frac{1}{\Gamma}})\gamma^{(0.17\Gamma - 0.81)} \tag{12}$$

where μ_F is foam viscosity, mPa·s; Γ is foam quality, %; γ is share rate, ms^{-1}.

2.4. Initial and Boundary Conditions

In order to solve the above mathematical model, the boundary conditions and initial conditions are as follows: Figure 1 shows the two-dimensional simulation area of the mathematical model.

$$C_f(x, y, t)|_{t=0} = 0 \tag{13}$$

$$\phi_{x,y,t=0} = \phi_0 \tag{14}$$

$$C_f(x, y, t)|_{x=0} = C_0 \tag{15}$$

$$q = \int_0^H u_{x,y} dy|_{x=0} = q_0 \tag{16}$$

$$u_{x,y=0} = 0, v_{x,y=0} = 0 \tag{17}$$

$$u_{x,y=H} = 0, v_{x,y=H} = 0 \tag{18}$$

$$p_{x=L,y} = p_{\text{outlet}} = c \tag{19}$$

where φ_0 is the initial porosity value of porous medium in the mathematical model, %; C_0 is the injected acid concentration, kmol/m^3; q_0 is the injection rate, cm^3/s; P_{outlet} means outlet pressure, MPa; c is a constant.
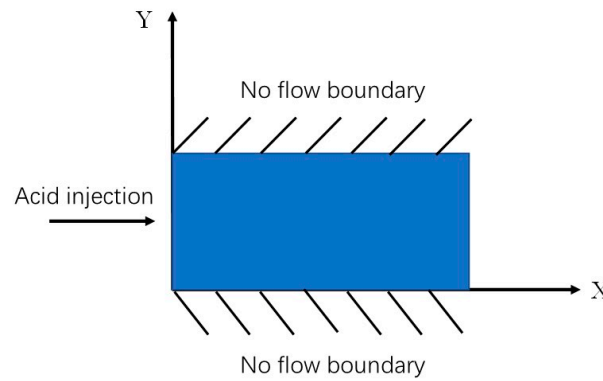
Figure 1. Simulation domain of 2D model.

2.5. Model Discretization and Implementation

In order to solve the above mathematical models, each model needs to be discretization. Due to the fact that the calculation is carried out in a two-dimensional plane, the flow in the z-direction is temporarily not considered for each equation. Considering the good conservation and grid adaptability of the finite volume method, this method is used for differential dispersion. As shown in Figure 2, it is a schematic diagram of grid division for differential dispersion.
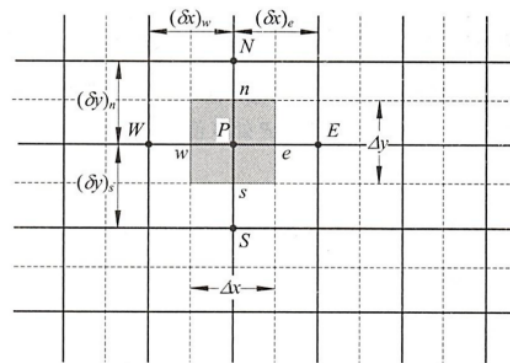
Figure 2. Schematic diagram for 2D coordinate grid.

Based on the dispersion of equation differences in the above mathematical model, C++ programming is used to calculate and solve under the set initial and boundary conditions. Design a solution flowchart based on the solution and research ideas, as shown in Figure 3.
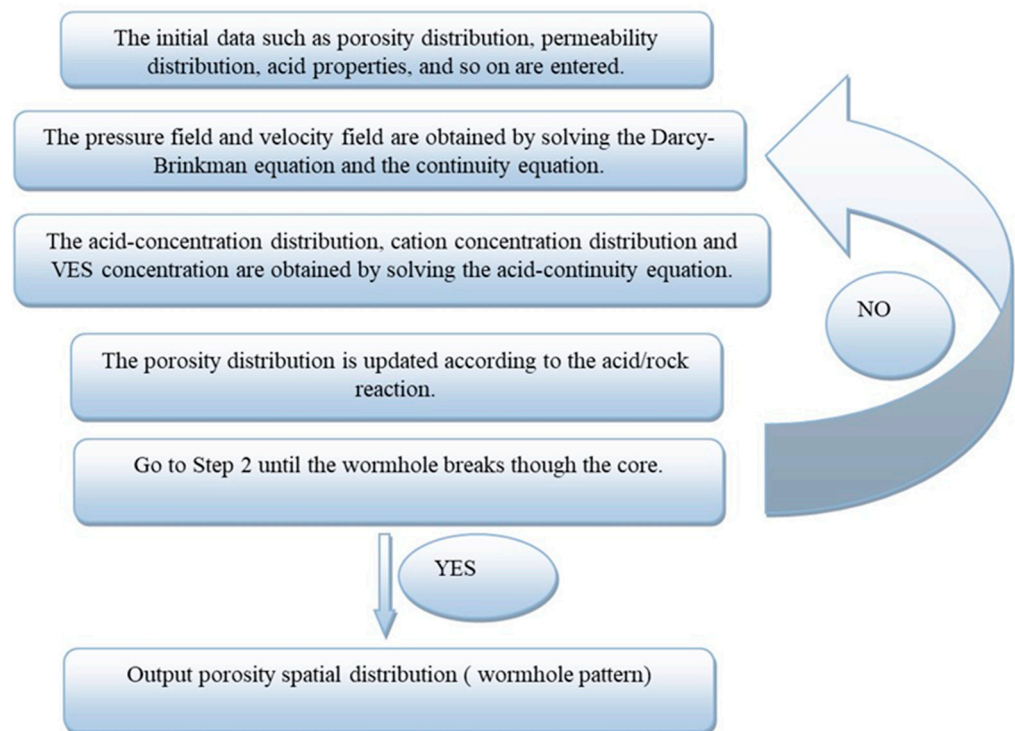
Figure 3. The workflow of mathematical model solution.

3. Results and Discussion

Utilizing the mathematical model established above, a comprehensive numerical simulation of the acidification process of foamed-VES acid in cores is conducted by coupling with the distribution of matrix pore space. Through this simulation, the propagation behavior of wormholes caused by the etching of foamed-VES acid is studied, including the impact of factors such as reservoir heterogeneity, injection velocity, foam quality, and model dimensions on the propagation process. The model parameters used in this study are summarized in Table 1.

Table 1. Simulation parameters and values in wormhole propagation model.

Parameters and Units	Value	Parameters and Units	Value
Length, m	0.065	Initial pore radius, m	6×10^{-8}
Width, m	0.025	α, g/mol	30
Reaction rate constant $\text{mol}/(\text{m}^2 \cdot \text{s} \cdot (\text{mol}/\text{m}^3)\, \gamma^{(1)})$	0.001	Density, kg/m^3	2650
Diffusion coefficient m^2/s	1.2×10^{-9}	Acid concentration, wt%	15%
Foam quality, %	75, 85, 95		

3.1. Effect of Injection Rate

Based on the research of the literature, the injection rate has a significant impact on the propagation of acid-etched wormholes. However, due to limitations such as equipment accuracy and pump displacement, actual core acidification flow experiments cannot be conducted for both low and high injection rates in the laboratory. As such, it is necessary to conduct numerical simulations to investigate the propagation behavior of foamed-VES acid-etched wormholes under different injection rates and explore the optimal injection rate to enhance acidification efficiency and guide on-site acidification operations. Figure 4 shows the acid dissolution patterns under different injection rates. It can be seen that the influence of the injection rate is evident in the acid dissolution pattern, which can

be categorized into five types: surface dissolution, conical-shaped wormhole, dominant wormhole, ramified wormhole, and uniform dissolution.
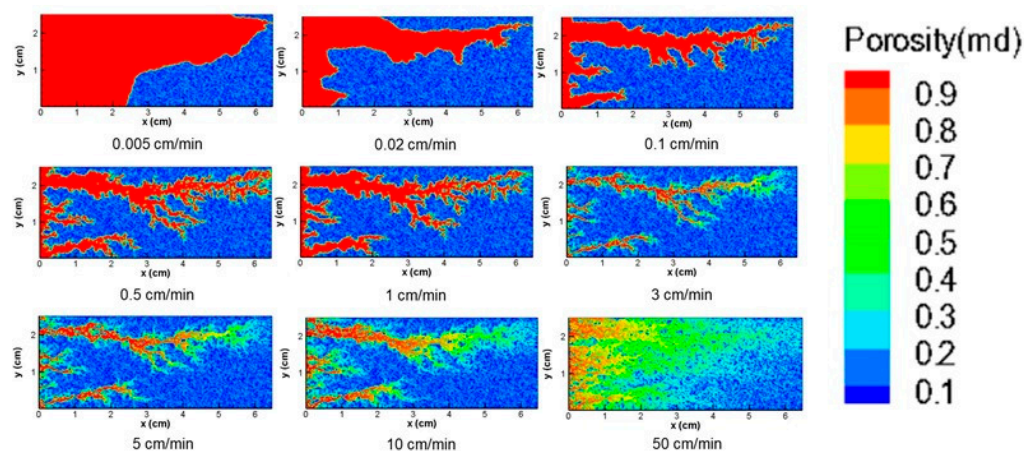
Figure 4. Acid dissolution pattern changes with injection rate.

At a low injection rate of 0.05 cm/min, the acid solution advances uniformly in the rock core, dissolving almost all of the reservoirs in its path. As the acid injection continues, the random distribution of pore media in the reservoir causes the accumulation of more acid in the upper part of the core, accelerating the acid's advance in that area until it breaks through the entire core. As the injection rate increases, the acid dissolution pattern shifts from face dissolution to a conical wormhole, resulting in an appropriate increase in acidizing efficiency. When the injection rate is further increased to 3 cm/min, the mass transfer velocity and surface reaction rate are on the order of unity. Ultimately, the core is penetrated in the form of a dominant wormhole, which consumes less acid solution volume with high acidizing efficiency. Furthermore, at injection rates of 50 cm/min or higher, the acid dissolution pattern differs from the previous cases. The acid solution disperses throughout the entire core, similar to a mist, resulting in a typical uniform dissolution mode.

By analyzing the propagation pattern of acid wormholes under different injection rates, it is found that the dissolution pattern of foamed-VES acidizing is the same as that of existing acids, such as hydrochloric acid, thickened acid, and VES acid. As the injection rate gradually increases, the erosion mode changes from surface dissolution to conical wormholes, then to dominant wormholes, ramified wormholes, and, finally, to uniform dissolution. Therefore, there is still an optimal injection rate for foamed-VES acidizing, which is typically obtained by plotting the relationship between the injection rate and the volume of acid breakthrough. Figure 5 shows the relationship between injection rate and PVbt for foamed VES. It can be seen from the figure that the optimal injection rate range is between 1 cm/min and 5 cm/min. When the injection rate is lower than the optimal rate, more acid volume is consumed as the speed decreases. When the injection rate is higher than the optimal rate, the consumed acid volume increases with the speed, but the growth trend changes sharply to slow.
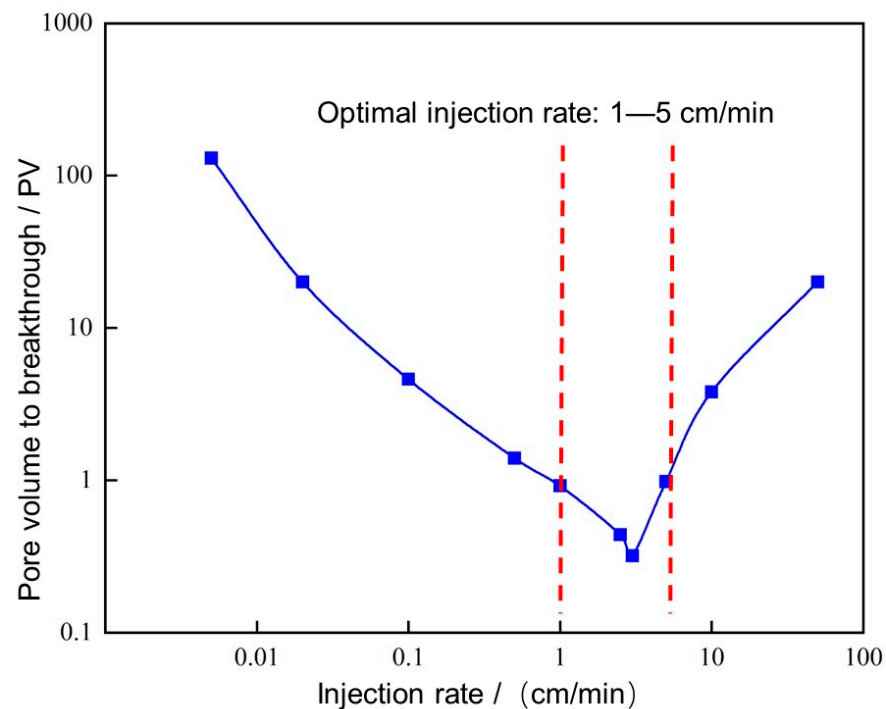
Figure 5. The relationship curve between injection rate and PVbt.

3.2. Effect of Formation Heterogeneity

Due to the strong heterogeneity of carbonate reservoirs, it is crucial to investigate the impact on the propagation of foamed-VES acid wormholes. This section primarily focuses on two aspects: the different porosity distribution patterns and initial permeability.

3.2.1. Porosity Distribution Patterns

Porosity is defined as the ratio of the pore volume of rock in a reservoir to the total volume of the rock. Obviously, not all pores are effective pores, and disconnected pores do not contribute to production. However, these disconnected pores have a certain impact on foamed-VES acidizing. Therefore, there are differences in the porosity distribution patterns generated by different simulation methods. It is necessary to conduct in-depth research on whether these different porosity distribution patterns affect the propagation of foamed-VES acid wormholes. Currently, most scholars simulate reservoir porosity distribution using two methods: artificially generated random porosity distribution and spatially correlated porosity distribution [11]. Mou Jianye et al. obtained the real rock core pore space distribution through CT scanning and used it for the numerical simulation of acid wormhole propagation [25]. Therefore, the impact of porosity distribution generated by the above three methods on the propagation pattern of foamed-VES acid wormholes needs to be studied.

As mentioned above, the optimal injection rate range for foamed-VES acidizing is from 1 cm/min to 5 cm/min. Therefore, numerical simulations were conducted using an injection rate of 2.5 cm/min while holding other parameters constant. Figure 6 shows the acid wormhole morphology under different porosity distribution patterns. Figure 6a shows the final acid wormhole morphology under a random porosity distribution pattern. It can be seen that multiple wormholes grow and develop simultaneously at the initial stage. After competing with each other, only three wormholes continue to grow and extend, and one of them breaks through the rock core with an absolute advantage in propagation. This wormhole consumes 0.44 PV of acid fluid during core breakthrough, and the dissolution mode is a typical dominant wormhole morphology. Figure 6b shows the final acid wormhole morphology under a spatially correlated porosity distribution pattern, where the extension and propagation of wormholes are similar to those under a

random porosity distribution pattern. Similarly, at the initial stage, multiple wormholes grow and extend simultaneously, and a few wormholes continue to expand after competing for advantages. However, as porosity distribution has some correlation in the X-direction, which is favorable for acid flow in the X-direction, the dominant wormholes can extend and expand simultaneously instead of only one wormhole expanding until a breakthrough. Therefore, compared to the random porosity distribution pattern, the volume of acid fluid consumed during wormhole breakthrough increases significantly. Figure 6c shows the final acid wormhole morphology based on the actual rock core pore space distribution. At the initial stage, only a few wormholes grow and extend simultaneously in areas with larger initial porosity, which is different from the growth pattern of wormholes under the other two distribution patterns. This is because the porosity distribution of the actual rock core is significantly more heterogeneous. As acid fluid is continuously injected, one wormhole gains an absolute advantage and extends forward after competing with others. Obviously, it will communicate with the areas with larger initial porosity during the extension process, thus changing the propagation path of the wormhole. Finally, this wormhole consumed 0.48 PV of acid fluid during core breakthrough, and its dissolution mode was typical of a dominant wormhole morphology.
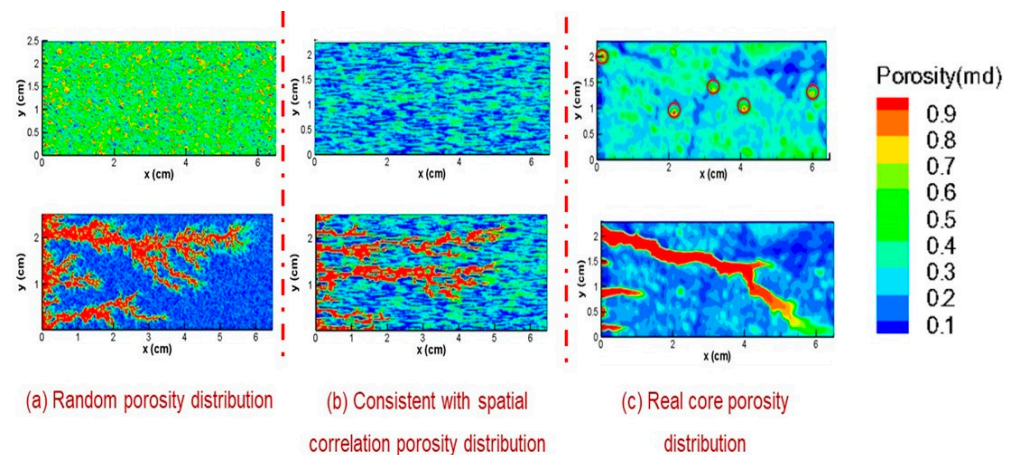
Figure 6. Different distribution form of porosity and corresponding acid-etched wormhole form.

Furthermore, the final acid-etched wormhole morphology under the random porosity distribution pattern is similar to that of the actual rock core, and the PVbt is also close. Accordingly, it is reasonable to use the random porosity distribution pattern for numerical simulation of the propagation of foamed-VES acid wormholes.

3.2.2. Initial Permeability

The initial permeability used for numerical simulation is the average permeability of the modeling area, and its value has a significant impact on wormhole propagation. To investigate this effect, different initial permeability models were generated using the open-source geostatistics software GLSIB. These models were then coupled with the wormhole propagation mathematical model to conduct numerical simulations of wormhole propagation. Figure 7 presents the resulting porosity-matrix models with initial permeabilities of 5 mD, 25 mD, and 50 mD, respectively. Other parameters were kept constant while numerical simulations of wormhole propagation were performed using 95% foam quality under various injection rates, and the acid volume required for wormhole breakthrough was calculated.
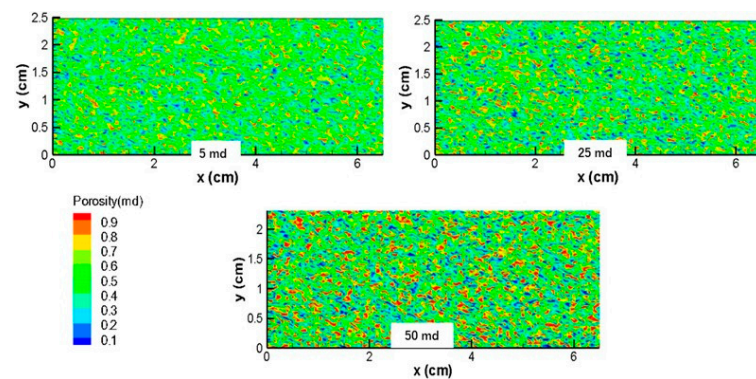
Figure 7. The models with different initial permeabilities.

Figure 8 displays the correlation between the injection rate and PVbt for different initial permeabilities. It is observed that, at the same injection rate, the PVbt decreases as the initial permeability increases. This is attributed to the fact that high-permeability rock cores also have higher porosity and excellent connectivity, which requires less acid volume for wormhole breakthrough under the same conditions. Furthermore, the optimal injection rate for foamed-VES acidification lies at 1–5 cm/min for various initial permeabilities of the rock cores, indicating that the initial permeability does not affect the optimal injection rate for similar rock cores.
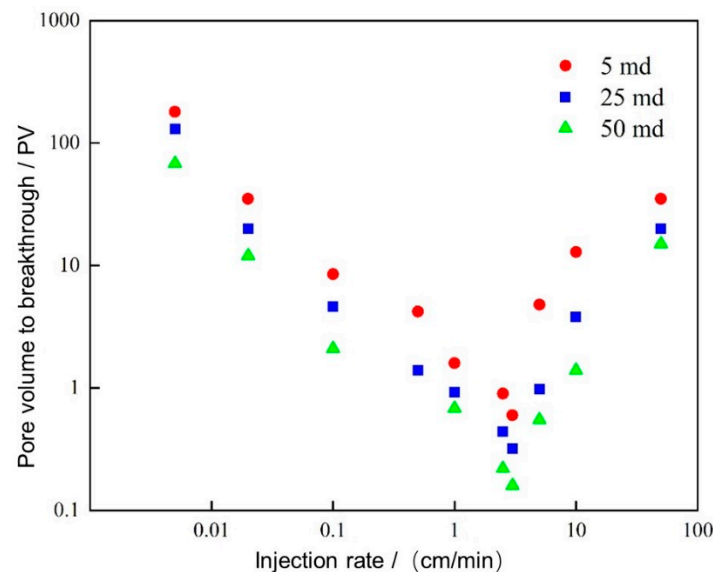
Figure 8. The relationship between injection rate and PVbt under different initial permeabilities.

3.3. Effect of Foam Quality

The foam quality is a critical parameter for the acid treatment of foamed VES. In field operation, the foam quality of the foamed-VES acid used typically exceeds 90%. Therefore, using foam masses of 95%, 85%, and 75%, respectively, while keeping all other parameters constant, numerical simulations of wormhole propagation were conducted to investigate the impact of foam quality on the acidification behavior of foamed VES. VES acid was also included in the simulations as a control experiment.

Figure 9 shows the morphology of the acid-etched wormholes of VES acid and foamed-VES acid with varying foam quality at an injection rate of 1.5 cm/min. From the figure, it is evident that for VES acid, the final dissolution mode is conical pores, which results in a significantly higher consumption of acid and a more extensive erosion of the rocks when compared to foamed-VES acid with variable foam quality. Among the three foamed-VES acid solutions with varying foam quality, the propagation pattern and the final form of the

acid-etched wormhole are quite similar, and the wormhole with the upper-left corner's absolute advantage continues to extend until it breaks through the core. However, the relative advantage of the wormhole will develop longer and consume more acid solution for foamed-VES acid solutions with lower foam quality.
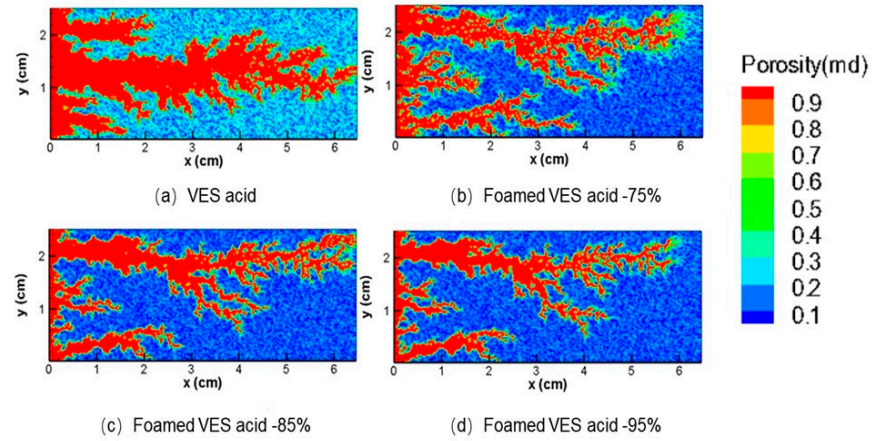
Figure 9. Acid-etched wormhole morphologies of VES acid and foamed-VES acid with different foam quality.

Figure 10 displays the correlation between PVbt and injection rate of VES acid and foamed-VES acid with different foam quality. It is clear from the figure that, at the same injection rate, VES acid consumes the highest amount of acid volume, which is consistent with the previously described final wormhole morphology. For foamed-VES acid with varying foam quality, the volume of acid required for breakthrough increases slightly as foam quality decreases. However, the increase is not significant, implying that reducing foam quality would not have a significant impact on the operation of acid pore volume multiples alone. Nevertheless, in practical acidification treatments, high foam quality is favorable for enhancing energy and strengthening the backflow of the acid solution, thereby improving the acidification performance and effectiveness.
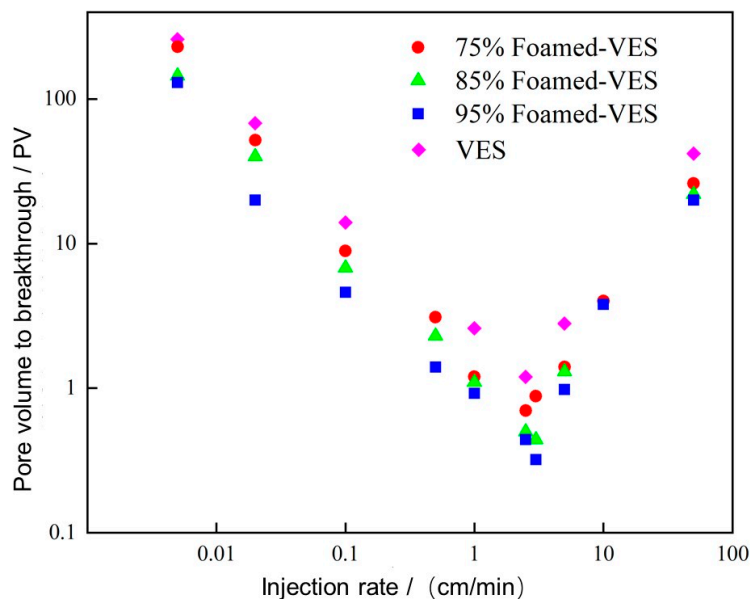
Figure 10. The relationship curve between injection rate and PVbt for VES acid and foamed-VES acid with different foam quality.

3.4. Effect of Model Dimension

The size of the simulation region has a notable impact on the acid wormhole propagation law for the two-dimensional linear foamed-VES acid mathematical model. In this regard, the chosen reference size was 2.5 cm × 6.5 cm, which was the same as the rock core size used in the acidification flow experiment and the model size utilized in the previous numerical simulation. To investigate the influence of region size, the model was expanded by increasing its length, width, or both simultaneously. In addition, it was important to maintain a consistent mesh size to eliminate its influence on the results.

Figure 11 displays the morphology of acid-etched wormholes in simulated regions of different sizes with an injection rate of 2.5 cm/min and foam quality of 95%. As the injection rate is close to the optimum injection rate for wormhole propagation, the dominant wormhole should theoretically form. The figure confirms this as the dominant wormhole morphology is observed in all sizes, verifying the previous conclusion. At the initial stage, multiple wormholes grow and extend simultaneously. However, with the continuous injection of acid, four wormholes gain an advantage and continue to expand until the top-left wormhole breakthrough occurs. When comparing Figure 8a,b, where the model width is held constant and the length is doubled, the wormhole growth patterns are consistent in the longitudinal direction, while other wormholes also grow longer in the transverse direction, except for the dominant wormhole. By comparing Figure 8a,c, where the model length is held constant and the width is doubled, the wormhole propagation laws are almost the same, indicating that the longitudinal changes have little effect on the propagation of acid-etched wormholes under the premise of a consistent porosity distribution. Likewise, for Figure 8b,d, where the length is held constant and the width is expanded by 5.2 times, the wormhole propagation law is consistent, further supporting the previous conclusion.

(a) 2.5 cm×6.5 cm (b) 2.5 cm×13 cm

(c) 5 cm×6.5 cm (d) 13 cm×13 cm
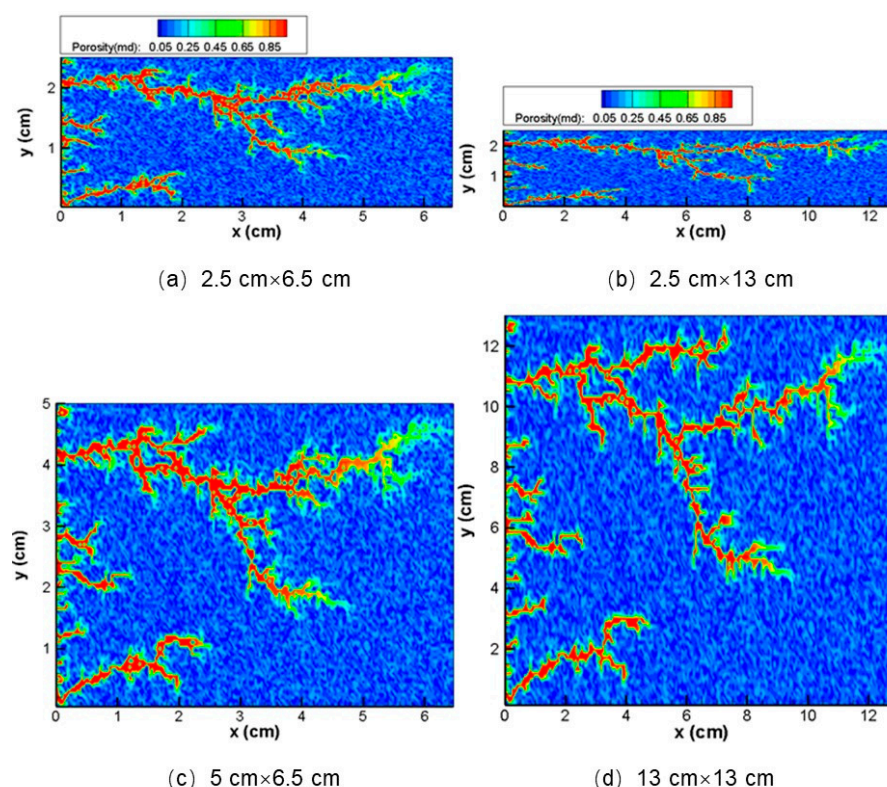
Figure 11. Acid-etched wormhole morphologies under different domain sizes.

Numerical simulations were performed at different injection rates using models of varying sizes, and the relationship between injection rate and PVbt is shown in Figure 12. Firstly, it can be observed from the figure that the optimum injection rate range remains nearly constant for the models of different sizes. Secondly, comparing models

a (2.5 cm × 6 cm) and c (5 cm × 6 cm), the curve shifts downward and to the right when the injection rate is below the optimum injection rate while holding the core length constant and increasing its width. The underlying reason is that as the core width increases, the pore volume must also increase. However, the volume of acid consumed changes only slightly, meaning that under low injection rate conditions, the PVbt is inversely proportional to the core width. When the injection rate is higher than the optimum value, the convection effect is far stronger than the diffusion effect, causing the acid solution to move to the far end without sufficient reaction time before breaking through the core, resulting in little change in the PVbt under high flow rate conditions. Likewise, comparing models b (2.5 cm × 13 cm) and d (13 cm × 13 cm), a similar trend is observed, again verifying the previous conclusion. When comparing models a (2.5 cm × 6 cm) and b (2.5 cm × 13 cm), where the width remains constant while the length doubles, it is clear that the PVbt consumed by the latter is always higher, regardless of whether the injection rate is below or above the optimum value. Although the length increases, the pore volume increases, and the amount of acid consumed to form wormholes also increases significantly. As a result, the PVbt presents an overall upward trend.
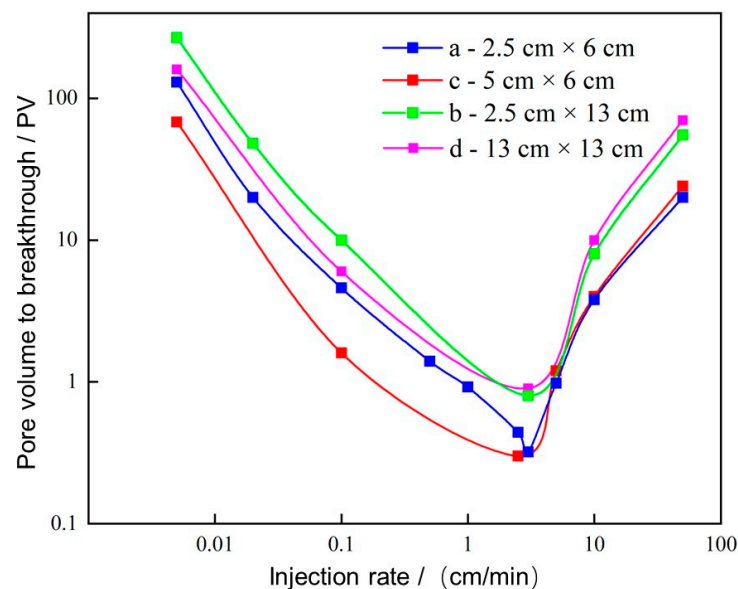
Figure 12. The relationship curve between injection rate and PVbt under different domain sizes.

3.5. Evaluation of Diversion Performance

To achieve successful acidizing in highly heterogeneous long horizontal well sections and thick carbonate reservoirs with numerous small layers, it is essential to ensure uniform acid distribution to enable effective stimulation of each layer or section, increase reservoir productivity, and improve oil and gas well production. Therefore, it is crucial to conduct numerical simulations to investigate the temporary plugging and steering abilities of foamed-VES acid.

Based on the research of the literature, it is known that VES acid becomes ineffective when the permeability contrast is over 10. Therefore, for the numerical simulation of foamed-VES acid parallel acidification, a reference group with a permeability contrast of 10 was selected. Different permeability contrasts of 15 and 20 were also employed to explore the performance of the acidizing process.

Figure 13 displays the final acid wormhole morphology in high- and low-permeability reservoirs during general acidizing using foamed-VES acid and VES acid under different permeability levels. During the acidizing treatment of VES acid, the acid solution preferentially enters the layer with low seepage resistance, and the high-permeability layer is preferentially transformed. As the acid rock reaction produces Ca^{2+} ions, VES forms wormlike micelles, sharply increasing the viscosity of the acid solution and forcing the

subsequent acid solution to turn towards the low-permeability layer. This self-viscosifying property of VES facilitates uniform acid distribution. However, the initial permeability difference of the reservoir can cause acid fluid to flow into the high-permeability layer, and the stimulated degree of the low-permeability layer depends on the relative strengths of VES's self-viscosity increasing effect and the permeability contrast effect.
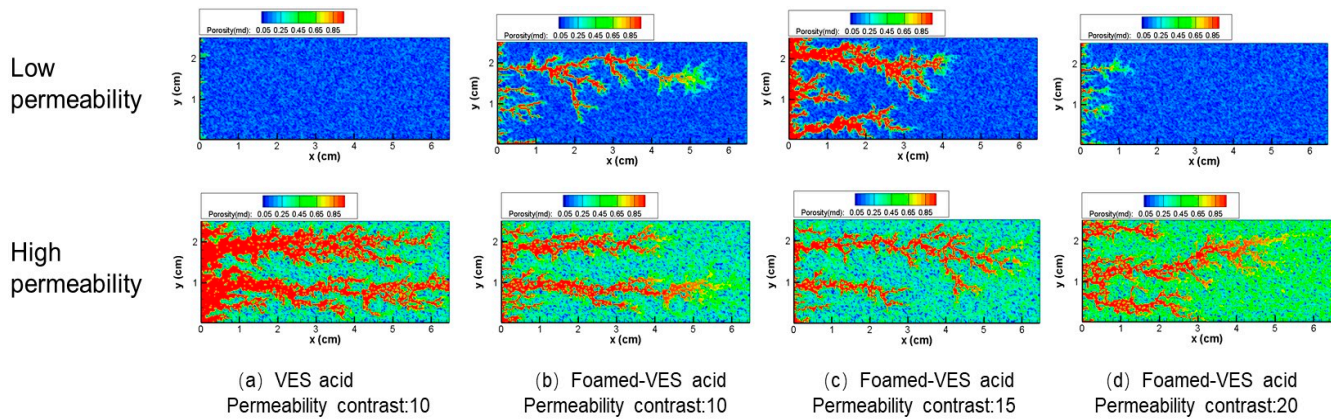
Figure 13. Effect of uniform acid distribution for foamed VES and VES acid under different initial permeability contrast.

Figure 13a shows the development of acid wormholes in high- and low-permeability reservoirs during general acidizing with VES acid under the condition of a permeability contrast of 10. The image shows that the low-permeability layer has hardly been modified, while the high-permeability layer has formed a large number of wormholes, resulting in unnecessary waste of acid. This occurs because the initial permeability difference is too large for the VES acid viscosity-increasing property to steer subsequent acid liquid toward the low-permeability layer. Consequently, diversion takes place in the high-permeability layer, causing it to undergo transitional transformation. The numerical simulation results again confirm the view previously put forward by predecessors that VES acid has no diversion effect when the permeability contrast is 10. Additionally, it should be noted that in the case of a large permeability difference, VES acid may not improve the transformation effect and may instead reduce the acidizing efficiency. Therefore, for reservoirs with repeated acidizing or strong heterogeneity, VES acidification should be avoided to prevent unnecessary acid waste.

Figure 13b displays the development of acid wormholes in high- and low-permeability reservoirs during general acidizing using foamed-VES acid under the condition of a permeability contrast of 10. It is evident from the image that wormholes eventually penetrate the high-permeability reservoir, while main wormholes are also developed in the low-permeability reservoir. This suggests that under such a permeability difference, foamed-VES acid has good temporary plugging and diversion effects, enabling uniform acid distribution. When the permeability contrast is further increased to 15, the acid wormhole morphology in high- and low-permeability reservoirs is shown in Figure 13c. Even with such a high permeability difference, the acid-etched wormholes in the low-permeability rock core still extend about 70% of the core length. As the initial permeability contrast is further increased to 20, the acid wormhole morphology in high- and low-permeability reservoirs is shown in Figure 13d. The acid wormhole evidently still penetrates the high-permeability rock core, but the wormhole in the low-permeability rock core is relatively short, indicating that the temporary plugging and steering effect of foamed-VES acid is greatly reduced, but there is still some steering capability.

4. Conclusions

Based on the mathematical model of foamed-VES acid-etched wormhole propagation, various influencing factors such as the injection rate, reservoir heterogeneity, foam quality,

and simulation region size were studied to investigate their effects on the propagation pattern of foamed-VES acid-etched wormholes. The following conclusions were reached:

(1) The optimal injection rate range for foamed-VES acid is between 1 and 3 cm/min. The dissolution mode of foamed-VES acid aligns with conventional hydrochloric acid and VES acid. As the injection rate increases, the acid solution progresses through various dissolution modes, such as surface dissolution, conical wormholes, dominant wormholes, ramified wormholes, and uniform dissolution.

(2) Simulated foamed-VES acid-etched wormhole propagation with an artificially randomized porosity distribution more closely approximates actual core acidizing results.

(3) For a given pore matrix model, the initial permeability does not impact the optimal injection rate of foamed-VES acidizing. Furthermore, as permeability increases, the pore volume multiple of acid fluid consumed decreases.

(4) At the optimal injection rate, the foam quality has a minor effect on the morphology of acid wormholes, but it can impact the pore volume multiple of acid consumed. Higher foam quality results in lower acid volume consumption and increased energy, which in turn can strengthen flowback.

(5) The optimization study reveals that the optimal injection velocity range is unaffected by variations in the simulated area size.

(6) The results indicate that VES acid lacks the ability to achieve diversion when the initial permeability contrast is over 10. However, the foamed-VES acid demonstrates a certain temporary plugging and diverting ability when the permeability contrast is 20.

Data Availability Statement: Not applicable.

Conflicts of Interest: The authors declare no conflict of interest.

References

1. EIA. *Annual Energy Outlook 2018*; U.S. Energy Information Administration: Washington, DC, USA, 2022.
2. Zhang, L.; Zhou, F.; Feng, W.; Pournik, M.; Li, Z.; Li, X. Experimental study on plugging behavior of degradable fibers and particulates within acid-etched fracture. *J. Pet. Sci. Eng.* **2020**, *185*, 106455. [CrossRef]
3. Zhang, L.; Zhou, F.; Zhang, S.; Li, Z.; Wang, J.; Wang, Y. Evaluation of permeability damage caused by drilling and fracturing fluids in tight low permeability sandstone reservoirs. *J. Pet. Sci. Eng.* **2019**, *175*, 1122–1135.
4. Zhang, L.; Zhou, F.; Mou, J.; Pournik, M.; Tao, S.; Wang, D.; Wang, Y. Large-scale true tri-axial fracturing experimental investigation on diversion behavior of fiber using 3D printing model of rock formation. *J. Pet. Sci. Eng.* **2019**, *181*, 106171. [CrossRef]
5. McLeod, H.O. Matrix acidizing. *J. Pet. Technol.* **1984**, *36*, 2055–2069. [CrossRef]
6. Wang, L.; Mou, J.; Mo, S.; Zhao, B.; Liu, Z.; Tian, X. Modeling matrix acidizing in naturally fractured carbonate reservoirs. *J. Pet. Sci. Eng.* **2020**, *186*, 106685. [CrossRef]
7. Mou, J.; Yu, X.; Wang, L.; Zhang, S.; Ma, X.; Lyu, X. Effect of Natural Fractures on Wormhole-Propagation Behavior. *SPE Prod. Oper.* **2019**, *34*, 145–158. [CrossRef]
8. Zhang, L.; Zhou, F.; Mou, J.; Xu, G.; Zhang, S.; Li, Z. A new method to improve long-term fracture conductivity in acid fracturing under high closure stress. *J. Pet. Sci. Eng.* **2018**, *171*, 760–770. [CrossRef]
9. Qu, Z.; Qu, G.; Qi, N. Research progress in viscoelastic surfactant self-diverting acid fluid system. *Pet. Geol. Oilfield Dev. Daqing* **2011**, *18*, 89–92.
10. Liu, N.; Liu, M. Simulation and analysis of wormhole propagation by VES acid in carbonate acidizing. *J. Pet. Sci. Eng.* **2016**, *138*, 57–65. [CrossRef]
11. Liu, M.; Zhang, S.; Mou, J.; Zhou, F.; Shi, Y. Diverting mechanism of viscoelastic surfactant-based self-diverting acid and its simulation. *J. Pet. Sci. Eng.* **2013**, *105*, 91–99. [CrossRef]

12. Mou, J.; Liu, M.; Zheng, K.; Zhang, S. Diversion conditions for viscoelastic-surfactant-based self-diversion acid in carbonate acidizing. *SPE Prod. Oper.* **2015**, *30*, 121–129. [CrossRef]
13. Gomaa, A.M.; Cutler, J.; Qu, Q.; Kawiezel, K.E. Acid placement: An effective VES system to stimulate high-temperature carbonate formations. In Proceedings of the SPE International Production and Operations Conference & Exhibition, Doha, Qatar, 14–16 May 2012; Society of Petroleum Engineers: London, UK, 2012.
14. Al-Otaibi, M.A.; Al-Muntasheri, G.A.; Hussein, I.A.; Chang, F.F. Laboratory Evaluation of Viscoelastic Surfactant Acid Diversion for Carbonate Reservoirs. In Proceedings of the SPE Middle East Oil and Gas Show and Conference, Manama, Bahrain, 25–28 September 2011; Society of Petroleum Engineers: London, UK, 2011.
15. Smith, C.L.; Anderson, J.L.; Roberts, P.G. New diverting techniques for acidizing and fracturing. In Proceedings of the SPE California Regional Meeting, San Francisco, CA, USA, 6–7 November 1969; Society of Petroleum Engineers: London, UK, 1969.
16. Rossen, W.R.; Wang, M.W. Modeling foams for acid diversion. *SPE J.* **1999**, *4*, 92–100. [CrossRef]
17. Cheng, L.; Kam, S.I.; Delshad, M.; Rossen, W.R. Simulation of dynamic foam-acid diversion processes. *SPE J.* **2002**, *7*, 316–324. [CrossRef]
18. Nguyen, Q.P.; Zitha, P.L.; Currie, P.K.; Rossen, W.R. CT study of liquid diversion with foam. *SPE Prod. Oper.* **2009**, *24*, 12–21. [CrossRef]
19. Letichevskiy, A.; Nikitin, A.; Parfenov, A.; Makarenko, V.; Lavrov, I.; Rukan, G.; Ovsyannikov, D.; Nuriakhmetov, R.; Gromovenko, A. Foam acid treatment-the key to stimulation of carbonate reservoirs in depleted oil fields of the Samara region. In Proceedings of the SPE Russian Petroleum Technology Conference, Moscow, Russia, 16–18 October 2017; Society of Petroleum Engineers: London, UK, 2017.
20. Li, S.; Li, Z.; Lin, R. Mathematical models for foam-diverted acidizing and their applications. *Petrol. Sci.* **2008**, *5*, 145–152. [CrossRef]
21. Li, Z. *Foam Fluid Application in Oil and Gas Exploitation*; Petroleum Industry Press: Beijing, China, 2010.
22. Panga MK, R.; Ziauddin, M.; Gandikota, R.; Balakotaiah, V. A new model for predicting wormhole structure and formation in acid stimulation of carbonates. In Proceedings of the SPE International Symposium and Exhibition on Formation Damage Control, Lafayette, LA, USA, 20–21 February 2004; Society of Petroleum Engineers: London, UK, 2004.
23. Brinkman, C. A calculation of the viscous force exerted by a flowing fluid on a dense swarm of particles. *Appl. Sci. Res. Sect. A Mech. Phys. Math.* **1947**, *1*, 27–34. [CrossRef]
24. Okpobiri, G.A.; Ikoku, C.U. Volumetric Requirements for Foam and Mist Drilling Operations. *SPE Drill. Eng.* **1986**, *1*, 71–88. [CrossRef]
25. Mou, J.; Li, S.; Zhao, X. Numerical Simulation Study on the Expansion Law of Acid-etched Wormholes Based on Real Pore Space Distribution. *Sci. Technol. Eng.* **2014**, *14*, 40–46.